Using elongated microparticles to enhance tailorable nanoemulsion delivery in excised human skin and volunteers

Miko Yamada[a,b], **Hossam Tayeb**[c,i], **Hequn Wang**[d], **Nhung Dang**[a,b], **Yousuf H. Mohammed**[e], **Sam Osseiran**[d,f], **Paul J. Belt**[g], **Michael S. Roberts**[e,h], **Conor L. Evans**[d], **Frank Sainsbury**[c,**], **Tarl W. Prow**[a,b,*]

[a]Future Industries Institute, University of South Australia, Adelaide, Australia

[b]Dermatology Research Centre, The University of Queensland, School of Medicine, Translational Research Institute at the Princess Alexandra Hospital, Brisbane, Australia

[c]Australian Institute for Bioengineering and Nanotechnology, The University of Queensland, St Lucia, Australia

[d]Wellman Centre for Photomedicine, Massachusetts General Hospital, Harvard Medical School, MA, USA

[e]Therapeutic Research Centre, School of Medicine, The University of Queensland, Princess Alexandra Hospital, Woolloongabba, Australia

[f]Harvard-MIT Division of Health Sciences and Technology, MA, USA

[g]Department of Plastic and Reconstructive Surgery and Orthopaedic Surgery, Princess Alexandra Hospital, Brisbane, Australia

[h]School of Pharmacy and Medical Science, University of South Australia, Adelaide, Australia

[i]Faculty of Applied Medical Sciences, King Abdulaziz University, Jeddah, Saudi Arabia

Abstract

This study demonstrates, for the first time, clinical testing of elongated silica microparticles (EMP) combined with tailorable nanoemulsions (TNE) to enhance topical delivery of hydrophobic drug surrogates. Likewise, this is the first report of 6-carboxyfluorescein (a model molecule for topically delivered hydrophobic drugs) AM1 & DAMP4 (novel short peptide surfactants) used in volunteers. The EMP penetrates through the epidermis and stop at the dermal-epidermal junction (DEJ). TNE are unusually stable and useful because the oil core allows high drug loading levels and the surface properties can be easily controlled. At first, we chose alginate as a crosslinking agent between EMP and TNE. We initially incorporated a fluorescent lipophilic dye, DiI, as a hydrophobic drug surrogate into TNE for visualization with microscopy. We compared four different coating approaches to combine EMP and TNE and tested these formulations

*Correspondence to: T. W. Prow, Medical Microtechnology Lab, Future Industries Institute, University of South Australia, Adelaide, SA 5001, Australia. **Correspondence to: F. Sainsbury, Australian Institute for Bioengineering and Nanotechnology, University of Queensland, St Lucia, Brisbane, QLD 4072, Australia, f.sainsbury@uq.edu.au (F. Sainsbury), tarl.prow@unisa.edu.au (T.W. Prow).

Supplementary data to this article can be found online at https://doi.org/10.1016/j.jconrel.2018.09.012.

in freshly excised human skin. The delivery profile characterisation was imaged by dye- free coherent anti-Stoke Raman scattering (CARS) microscopy to detect the core droplet of TNE that was packed with pharmaceutical grade lipid (glycerol) instead of DiI. These data show the EMP penetrating to the DEJ followed by controlled release of the TNE. Freeze-dried formulations with crosslinking resulted in a sustained release profile, whereas a freeze-dried formulation without crosslinking showed an immediate burst-type release profile. Finally, we tested the crosslinked TNE coated EMP formulation in volunteers using multiphoton microscopy (MPM) and fluorescence-lifetime imaging microscopy (FLIM) to document the penetration depth characteristics. These forms of microscopy have limitations in terms of image acquisition speed and imaging area coverage but can detect fluorescent drug delivery through the superficial skin in volunteers. 6-Carboxyfluorescein was selected as the fluorescent drug surrogate for the volunteer study based on the similarity of size, charge and hydrophobicity characteristics to small therapeutic drugs that are difficult to deliver through skin. The imaging data showed a 6-carboxyfluorescein signal deep in volunteer skin supporting the hypothesis that EMP can indeed enhance the delivery of TNE in human skin. There were no adverse events recorded at the time of the study or after the study, supporting the use of 6-carboxyfluorescein as a safe and detectable drug surrogate for topical drug research. In conclusion, dry formulations, with controllable release profiles can be obtained with TNE coated EMP that can effectively enhance hydrophobic payload delivery deep into the human epidermis.

1. Introduction

Delivery of drugs through the skin is an attractive, as well as, challenging area of research. On one hand, the skin is a highly accessible and convenient site for administration, yet on the other, its biophysical properties result in a barrier to many therapeutics and cosmeceuticals. In general, lipophilic compounds < 500 Da can penetrate the stratum corneum (SC) or traverse the epidermis through shunt pathways created by sweat glands and hair shafts. In contrast, delivery of larger molecules, such as peptides, proteins, siRNA, DNA or nanoparticles continues to be a major research challenge [1]. Efforts to develop safe and efficacious means of delivery across the skin continue to grow, thus furthering our understanding of percutaneous drug penetration, diffusion and permeation. However, the topical drug market still remains limited to a narrow range of permeable drugs despite evolving formulation approaches and chemical enhancers [2]. An additional challenge is that the skin's morphology and response to chemical/physical stimulus changes significantly based on age, body-site or disease state. For example, skin diseases such as psoriasis and skin cancer (including its precursor, actinic keratosis) present in thickening of the stratum corneum (SC) from 10–20 μm to 140–500 μm as a result of hyperkeratinisation.

Technologies have been developed to overcome this significant barrier including sonophoresis, laser and or thermal ablation, electroporation, radiofrequency treatment, iontophoresis, magnetophoresis, high pressure jets, and microneedle arrays [3]. Some of these techniques have been FDA-approved for topical and transdermal drug delivery. However, physical disruption may cause irritation, tingling and burning sensations. In some cases, long term damage to the skin barrier may be present. Alternatively, chemical enhancers such as fatty acids, surfactants, esters, polyalcohols and phospholipids can be

used to enhance topical drug penetration but using this approach for larger molecules and nanoparticles is problematic. This is because a much higher dosage, possibly toxic levels, of the chemical enhancer is required to achieve a pharmacologically effective delivery enhancement [3]. For this reason, the use of chemical enhancers has been limited and there is a need to balance improved skin permeability with drug- or disruption-related skin irritation.

An accepted and safe approach for delivering drugs to the skin is by integrating them in a nanoemulsion. The term nanoemulsion refers to a fine oil-in-water, water-in-oil or bi-continual dispersion, stabilised by an interfacial film of surfactant molecules and having a droplet size on a nm scale [4]. They are thermodynamically stable and oil-in-water nanoemulsions in particular have various advantages as drug carriers. For example, they have a high loading capacity for hydrophobic molecules and can protect bioactive payloads against hydrolysis and oxidation. Sequestration and protection of cargos can improve bioavailability and controlled release of drugs potentially permitting smaller doses with fewer adverse effects. Nanoemulsions are also biodegradable and can be rendered into several dosage forms, like liquids, creams, sprays, gels, aerosols and foams. They have a safe history with established use in pharmaceutical and cosmetic formulations and can be administered by almost all available routes including parenteral, ocular, nasal, oral, topical and even aerosilization to the lung [5].

Recent advances in decoupling the formation of emulsions from subsequent functionalization have been made with the invention of tailorable nanocarrier emulsions (TNE) [6]. The surface-active designer peptide, AM1 [7], can be used to stabilize nano-sized emulsions in the presence of metal ions, which promotes peptide interaction *via* histidine residues and the formation of a cohesive interfacial film [8]. The resulting mechanically stable emulsions can then be surface-modified by the spontaneous integration of the related protein, DAMP4 [9], to which functional moieties can be genetically or chemically conjugated. For example, polyethylene glycol (PEG)-DAMP4 conjugates spontaneously integrate onto an AM1-stabilised interface projecting the hydrophilic PEG into the aqueous phase, imparting hydrodynamic stability and modifying surface charge [10]. The ability to readily tailor the oil-water interface presents an opportunity to explore the role of the surface properties of TNE in hydrophobic drug delivery and in controlling their interactions with delivery platforms.

We have developed a physical penetration enhancing approach using elongated microparticle (EMP) technology that penetrates to the dermal-epidermal junction for maximizing drug permeability within the epidermis. These EMP are unbound, thus distinct from microneedle arrays, and can be mixed with the drug followed by gentle massage into the skin without being restricted by application site or area [11,12]. The EMP penetrate to the dermal-epidermal junction during application, but do not appear to go beyond. We previously investigated the fate of these particles in volunteer skin and found that they moved up and out of the skin with the same timing as epidermal turnover [12]. This flexible technology platform has the potential to enhance cutaneous delivery of a wide range of payloads including small molecules, peptides, proteins, vaccines, nutraceuticals and cosmetics in addition to larger nano-/micro-particles [11–14].

Here, we show that EMP can be combined with TNE as a method for minimally invasive controlled release of hydrophobic molecules to the viable epidermis *in vivo*. Surface-optimised TNE were freeze-dried on the surface of EMP either alone or *via* pre-coating the EMP with crosslinked sodium alginate. To characterise the controlled drug delivery profile within skin, we utilised a hydrophobic fluorescent dye (DiI) as one model drug. The visualization of DiI by microscopy demonstrated the release profile of the drug model into the individual skin strata. However, this technique has some drawbacks. For example, external labelling is time-consuming, the dye molecule could dissociate from the TNE and there can be bleaching of fluorescent dye over time that may lead to inconsistency in characterisation. Therefore, in parallel we used coherent anti-Stokes Ramen scattering (CARS) microscopy for characterizing delivery in living human skin. CARS is a label-free vibrational imaging technique that allows mapping and quantifying molecules based on their characteristic intrinsic vibrational contrasts [15]. We observed a relatively uniform and continuous delivery profile of both DiI and triglyceride in EMP treated areas within the epidermis. Then we applied EMP-TNE with a selected coating strategy to *in vitro* and *ex vivo* studies, followed by work in volunteers. We used 6-Carboxyfluorescein (CaF) in the core droplet of the TNE in volunteers for the first time. This fluorescent dye was imaged in volunteers with multiphoton microscopy (MPM) and fluorescence lifetime imaging microscopy (FLIM) for delivery depth characterisation at 2 time-points (15 min and 50 min) post application and delivery quantification at each depth at 30 min post application. The volunteer data shows the effective delivery of hydrophobic agent with EMP. Our coating strategy also shows the sustained release profile, which does correspond to our *ex vivo* study.

2. Material and methods

2.1. Material

AM1 (Ac-MKQLADSLHQLARQVSRLEHA-CONH2) was synthesized by Genscript (Piscataway, NJ, USA). Miglyol 812 was purchased from AXO Industry SA (Wavre, Belgium). 1,1′-Dioctadecyl-3,3,3′,3′-tetramethylindocarbocyanine perchlorate (DiI) was purched from Molecular Probes (Victoria, Australia). 4-(2-Hydroxyethyl)-1-piperazineethanesulfonic acid (HEPES) and zinc chloride ($ZnCl_2$) were purchased from Sigma-Aldrich (St Louis, MO, USA). mPEG-NHS (MW 5000, PDI < 1.08, purity > 95%) was purchased from Nanocs (Boston, MA, USA).

2.2. DAMP4 expression, purification and PEGylation

Expression and purification of DAMP4 was performed according to published methods [9]. Briefly, recombinant expression in *Escherichia coli* was driven by an inducible T7 promoter. Cell lysis and purification was performed using fast protein liquid chromatography. DAMP4 concentration was determined by high performance liquid chromatography and lyophilised. To prepare PEGylated DAMP4 (PEG-DAMP4), lyophilized DAMP4 was dissolved in HEPES (25 mM, pH 7.0) and a weighed amount of mPEG-NHS was added to give a final mPEG:DAMP4 molar ratio of 20:1. The reaction was allowed to incubate at 4 °C for 16 h. PEGylation of DAMP4 was verified by SDS-PAGE, which showed > 50% PEGylation (data not shown) and the conjugate was used without purification.

2.3. Tailorable nanoemulsion preparation

To prepare the TNE core, lyophilized AM1 (400 μM) was dissolved in 980 μl HEPES (25 mM, pH 7.0) containing $ZnCl_2$ (800 μM). Miglyol 812, optionally containing DiI at 1 mg/ml, was added to give an oil volume fraction of 2% (v/v) and the mixture was homogenized using an ultrasonicator as previously described [10]. Using the same method and oil volume fraction, Myglyol 812, containing CaF at 2.5 mg/ml, was prepared for volunteer application. To prepare P20-TNE, AM1-stabilised emulsion was slowly added to an equal volume of 40 μM PEG-DAMP4 to give 20 μM final concentration of PEG-DAMP4 followed by 60 s of vigorous stirring. To prepare P200-TNE, AM1-stabilised emulsion was similarly added to an equal volume of 400 μM PEG-DAMP4 and mixed.

TNE size and zeta potential were measured using a Malvern Zetasizer Nano ZS (Malvern, Worcestershire, UK). Data analysis was with DTS software (Malvern, version 6.2), using a non-negatively constrained least squares (NNLS) fitting algorithm. For each sample, 10 measurements of 10 s were performed in duplicate.

2.4. Elongated microparticle and applicator fabrication

The EMP were fabricated by micro-chopping, laser etching or deep reactive ion etching. Approximately 1 mm layer of 8 μm diameter silica oxide filament was processed to obtain 173.3 ± 100.8 μm EMP as previously described [11]. The length distribution was then measured using light microscopy followed by image analysis.

Autodesk Inventor Professional 2012 was used to model the applicator heads. The file was exported as a stereolithography (STL) file. The applicator was 3D-printed using a V-Flash FTI 230 Desktop Modeler (3D Systems, USA). The acrylic UV-crosslinking resin consisted of a proprietary V-Flash FTI-GN Material as previously described [11].

2.5. Elongated microparticle coating

Twenty-five mg of EMP was mixed with 50 μl of TNE by vigorous vortex in an Eppendorf tube. The suspension was left for 24 h at 4 °C. The supernatant was completely removed; EMP were then snap-frozen and freeze-dried under vacuum at −80 °C for 4–5 h. These samples were designated "Freeze dried".

Cross-linked samples were prepared by adding 1 ml alginate (0.5%) (Pronatal LF10/60, IMCD Australia limited, Victoria, Australia) mixed with 25 mg EMP by vortex and centrifuged at 6000 rpm for 5 min. The supernatant was removed and 500 μl of $CaCl_2$ (0.02%) was added. The mixture was left at 25 °C for 5 min and centrifuged at 6000 rpm for 5 min. The supernatant was removed, and 1 ml of Milli-Q water was mixed by vortex and then centrifuged to remove $CaCl_2$. This formulation is referred to as "alginate-coated –EMP". TNE (500 μl) was mixed with alginate-coated EMP by vortex and left at 25 °C overnight. The supernatant was completely removed and freeze-drying was performed as described above.

Coating release studies were conducted using an Olympus XM10 camera on an Olympus IX51 fluorescence microscope (Olympus, Australia). The coated EMP (1 mg) were attached to transparent diagnostic adhesive (3 M) film before imaging. The field was selected and

imaging began before saline application. Saline (100 µl) was then applied to the EMP and fluorescence images were taken at 2, 5, 10 and 20 min.

2.6. Ex vivo human skin treatment

Excised human skin from abdominoplasty was sourced from Greenslopes Hospital, Brisbane, Australia and approval was obtained from the University of Queensland Human Research Ethics Committee (Approval number: HREC_12_QPAH217) or was sourced from Massachusetts General Hospital (MGH), Boston, USA with approval obtained from Harvard University Human Research Ethics Committee (Protocol No: 2014P001345). Patients were healthy with no apparent skin conditions. The procedures were conducted in compliance with the National Health and Medical Research Council of Australia. Excessed adipose tissue was removed, followed by rinsing with saline. Excised human skin was used immediately, while viable or was stored at -20 °C for < 2 weeks until required. For frozen tissue, the skin was thawed, rinsed and the surface was gently patted until dried. The excised skin was pinned down on a cork-board maintaining slight/even tension across the surface. For TNE-EMP delivery, 50 µl of each formulation (described in Fig. 1), 0.9% saline (negative control) or TNE alone were placed onto the surface of the skin. Administration was achieved by massaging the payload mixture for 30 s using small circular motions within a 4 cm^2 circular area. To maintain consistency between administrations, an EMP applicator was used with an application force of 0.25 N. Negative control comparators were skin samples where all of the procedures were the same, except the TNE were absent. After administration, the payload was left on the skin for 30 min followed by removal of excess solution with cotton swabs. Skin was rinsed with water after treatment. The centre of the application area was excised using a 4 mm circular biopsy punch. A maximum of eight treatment groups were applied per piece of skin and biological triplicates were performed.

2.7. Microscopy and image analysis

Scanning electron microscopy (SEM) (JEOL JSM-6610LV, SEAL laboratory, USA) was performed to characterise the microstructure of TNE-EMP complex. Dry samples were placed on a carbo-coated copper grid. The SEM images were obtained with 5 Kv and 3,000× magnification.

The EMP and TNE delivery to *ex vivo* abdominal human skin was imaged with a confocal fluorescence microscope (Olympus FV1200, Japan), (excited at 750 nm for reflectance and at 550 nm for DiI).

The CARS microscope was built over a customized confocal microscope (Olympus FV1000, Center Valley, PA), which has an additional laser entry port to accept external light sources. CARS microscopy was performed using a dual output femtosecond pulsed laser system (Spectra-Physics Insight DeepSee, Santa Clara, CA), where the first output (pump beam) is tunable from 680 to 1300 nm, while the second (Stokes beam) is fixed at 1040 nm. To achieve lipid CARS imaging at the 2845 cm^{-1} band of CH$_2$, the 1040 nm output was chosen as the Stokes beam (ω_S), while the pump beam (ω_P) was set at 803 nm ($\omega_P - \omega_S = 2845$ cm^{-1}). A half-wave plate and a polarizer were placed at each of the two laser output ports to adjust the beam power. To focus the beams onto the sample, a

1.20 NA 60× water immersion microscope objective (Olympus UPLSAPO 60XW, Center Valley, PA) was used. CARS signal detection was achieved using both a short-pass and two band-pass filters (Chroma ET750sp-2p8, and HQ650/45× and HQ685/70 M, Bellows Falls, VT) placed in front of a thermoelectrically cooled photomultiplier tube (Hamamatsu H7422PA-50, Hamamatsu City, Japan). The total power of the two beams at the objective was ~25 mW for all experiments performed in this study.

2.8. Volunteer study

Three volunteers are recruited under the University of Queensland Human Research Ethics Committee (Approval number: HREC_12_QPAH217). Alginate coated EMP-TNE (P20) and TNE (P20) only were applied on different forearms to prevent cross contamination. One 2×2 cm^2 treatment area was marked on each forearm with a skin marker. Twenty milligrams of EMP-TNE formulation was applied for 30 s with an applicator and 20 μl of TNE was applied by using gloves and waited for 30 s. Then the treatment area was washed under the running water for 10 s to remove excess and the area was pat-dried. Multiphoton microscopy (MPM) was used to image the volunteers' treatment areas at 30 min post application by 40× objective. Fluorescence-lifetime imaging microscopy (FLIM) images of treated areas were collected to perform quantitative analysis of delivery. The volunteers were images at 15 min and 50 min-post application by MPM-FLIM with by a 10× objective.

2.8.1. MPM-FLIM—Multiphoton microscopy (MPM) was performed using the DermaInspect (Jen-Lab GmbH, Jena, Germany) equipped with an ultrashort (85 fs pulse width) pulsed mode-locked 80-MHz titanium sapphire laser (MaiTai, Spectra Physics, Mount View, California). The excitation was set to 900 nm for CaF and 800 nm for both second-harmonic generation (SHG) and autofluorescence signals, with an emission signal range of 350 to 650 nm established through the use of a BG39 bandpass filter (BG39, Schott glass color filter, Schott MG, Mainz, Germany). Images were recorded with water-immersion 10× or oil-immersion 40× objectives (Carl Zeiss, Germany). The laser power was set to 40 or 65 mW for 10× and 40× objective imaging, respectively, and the acquisition time for obtaining the images was 6.4 s per frame.

For FLIM, a time-correlated single-photon counting (TCSPC) SPC-830 detector (Becker & Hickl, Berlin, Germany) was incorporated into the MPM system. The TCSPC module constructs a time-resolved distribution of photon arrival times, known as a fluorescence decay trace across the x and y coordinates of the scan area. Fluorescence emission was spectrally resolved between linearly arranged photon counters through the use of dichroic filters in the beam path. The emission light was collected spectrally in a channel from 350 nm to 450 nm at 760 nm excitation for NADH, 800 nm excitation for NAD(P)H and collagen, and 900 nm excitation for TNE.

2.9. Statistical analysis

Statistical analysis was conducted using GraphPad Prism 6 software (GraphPad Software Inc. USA).

2.9.1. CARS microscopy image analysis—Image stacks were analyzed using Image J Software (NIH, USA). The reflectance confocal image stacks were used to characterise EMP that penetrated skin and their penetration depth. The EMP were distinguished by low intensity bordering resulting in their unique rectangular appearance compared to the surrounding tissue. The lipid signal was derived by subtracting the signal attributed to the 1040 nm image from the 803 nm image.

2.9.2. FLIM image analysis—In order to separate the fluorescence of the fluorescein label from that of the endogenous tissue autofluorescence, the FLIM images (10×) acquired with 800 nm excitation and 450–620 nm emission were analyzed using a custom image processing algorithm developed in Matlab (The °associated with each pixel of each FLIM image was transformed into a phasor with coordinates (G,S), where G and S respectively correspond to the real and imaginary components of the Fourier transform of the decay trace evaluated at the laser repetition frequency. Performing this operation over a homogenous image generates a two-dimensional cluster in phasor space; in the case of a heterogeneous image containing two sources of fluorescence, the resulting phasor cluster is distributed principally along the axis joining the two reference clusters. Given the broad phasor cluster resulting from the observed tissue fluorescence (predominantly arising from the various bound and unbound NAD(P)H and FAD coenzymes present in skin), a non-Euclidean separation approach was used, where the Mahalanobis distances between a given phasor and the reference clusters were evaluated to best estimate the fractional contributions of both tissue autofluorescence and the fluorescein label to the total fluorescence signal. To this aim, the TNE only samples were used as the endogenous reference for the image processing algorithm, while a pure sample of the labelled EMP was used as the exogenous reference. In this manner, the fractional contribution of fluorescein, *i.e.* a value bound between 0 and 1, was calculated for each pixel of each image from each volunteer; multiplying these values on a pixel-by-pixel basis with the raw photon count images from the FLIM data and averaging over the field of view thus yields a mean number of exogenous photons per image pixel for each volunteer.

3. Results

3.1. Characterisation of tailorable nanoemulsions, coating efficiency onto elongated microparticles and in vitro release

DiI was encapsulated within the oil phase as a model hydrophobic molecule to characterise the EMP-enhanced delivery profile of TNE. Initially, we prepared three TNE formulations consisting of AM1 alone or with PEG at varying concentration resulting in different densities of PEG displayed on the oil droplet surface. The average size of the particles was 173.9 ± 2.4 nm, 175.1 ± 1.7 nm and 179.2 ± 4.2 nm for AM1, P20 and P200, respectively. Their corresponding surface charge decreased with increased PEG loading resulting in 52.5 ± 1.1 mV, 47.3 ± 1.5 mV and 38.6 ± 1.2 mV for AM1, P20 and P200, respectively (Fig. 1A). The ability of the TNE to retain dye was then assessed over 5 days in solution. AM1 resulted in immediate DiI release and continued to release dye to 4% of the initial amount by day 5, which correlated with an increase in particle size, likely due to coalescence (data not shown). In contrast both P20 and P200 TNE remained stable and retained over 90% of DiI

over the 5 days (Fig. 1B). Given the significant loss of dye from the AM1 TNE and its lack of structural stability, it was excluded from the remainder of the study.

Next, we coated the P20 and P200 TNE onto the surface of EMP in the presence of cross-linked alginate or without alginate. Initial tests in the absence of freeze-drying showed that surface density of PEG on TNE affected the association of TNE with EMP, with the more positively charged P20 formulation adhering greater than P200 (data not shown). We also noted that drying the emulsion onto the EMP resulted in more efficient coating of resuspended EMP. Prior to coating we characterized particle size to determine any change due to the alginate vehicle and found that unbound TNE showed ± 4.07 nm (SE) in size irrespective of the presence of alginate after dry coating and release (Fig. 1C). However, the presence of negatively charged alginate improved EMP coating with highly positively charged P20 TNE resulting in mean of 98% coverage ($+/- 8.5\%$ SE) of EMP as measured by the % continuity of CARS signal around the periphery of the particles (Fig. 1D).

SEM and CARS were then used to visually characterise the EMP coatings. The alginate P20 and P200 formulations resulted in a similar appearance with relatively uniform surface morphology of the EMP, which are then surrounded by excess excipient (Fig. 2A&B). The TNE coatings without alginate also resulted in a relatively rough, discontinuous surface coating.

CARS imaging was done to verify that TNE formulations were on the EMP surface by evaluating lipid specific signals originating from the surface of coated EMP. The P20-alginate coated EMP resulted in the highest signal followed by P200-alginate, P20 and P200 formulations. The two alginate formulations resulted in more uniform coverage of signal between EMP. This was in contrast to the two formulations without alginate where some EMP resulted in greater signal than others. These results agree with the quantitative measurements in Fig. 1D where P20-alginate resulted in high signal with low variation compared to the formulations without alginate that had a greater degree of variability.

We visually evaluated the *in vitro* release profiles of the P20 and P200 dry formulations containing DiI as a fluorescent surrogate for the TNE payload in Fig. 3. The fluorescence images supported the SEM and CARS data above. Both TNE types were dry coated onto EMP using freeze-drying or cross-linked alginate. All formulations showed intense fluorescence across the EMP, with EMP coated with P20 TNE and alginate having the most intense overall coating. The EMP coated with P20 TNE and alginate also showed bright spots suggesting areas of thicker coating or areas of TNE accumulation. There were obvious differences in the morphologies of the coating after PBS was added to the EMP. The EMP coated with P20 TNE that were freeze-dried showed an instantaneous decrease in fluorescence intensity that suggested most of the formulation was removed in < 2 min. There were also large, intensely fluorescent aggregates that did not change in size or intensity over 20 min. The EMP coated with P20 TNE using alginate showed a slower release profile that appeared to last over 20 min. The EMP coated with both P200 TNE formulations did not show any obvious differences over the time course. In a separate experiment we evaluated 24 and 48-h time courses but did not observe any consistent release differences between the groups (data not shown). These data supported our hypothesis that the major differences in

release profiles take place at < 24 h. Therefore, based on these results the alginate-coated EMP with TNE (P20) was used for the remaining studies.

3.2. Delivery and distribution of hydrophobic dye (DiI) in excised human skin

The delivery profile of TNE encapsulated DiI was assessed within excised thawed human skin using confocal microscopy. The DiI formulation without EMP resulted in the majority of dye accumulation on the surface of the skin (Fig. 4). More specifically, DiI signal was observed in the skin furrows and surrounding the corneocytes. As depth increased, DiI signal diminished from around the cells and was only observed in the skin furrows. The EMP enhanced TNE formulation without alginate resulted in enhanced depth of delivery compared to TNE alone (Fig. 4). The distribution of DiI differed, with the dye resulting in a more uniform profile across the administration area with EMP enhancement compared to the TNE alone group. The signal was visually more intense in the TNE + EMP freeze dried group in areas near the skin surface, *i.e.* < 15 μm deep, than the other groups. However, the TNE alginate group with EMP showed increased delivery > 15 μm (Fig. 4). Image analysis of the signal agreed with these observations (Fig. 5). Together, they show that we can selectively improve topical drug delivery to the uppermost 15 μm with one formulation (freeze-dried) and to the deeper viable epidermis with a second formulation (alginate crosslinking).

3.3. Enhanced Miglyol delivery to ex vivo live human skin

After confirming the successful penetration and delivery of DiI into living, excised human skin, TNE formulations were applied to skin and the distribution characterized over time using CARS microscopy (Fig. 6). Assessment of NAD(P)H signal showed a halo of low signal surrounding individual EMP that could indicate a single layer of ruptured cells or focal oedema (Fig. 6). Relatively little changes were observed in NAD(P)H signal after 30 min (data not shown). We observed that the Miglyol/TNE formulation is relatively non-toxic to keratinocytes to 0.04% (Fig. S1). Therefore, we hypothesize that the dark halo observed immediately around the EMP may be the result of mechanical disruption by the EMP during penetration. The NAD(P)H imaging supports this idea because the halo appears to be limited to a single cell layer.

We carried out live tissue CARS imaging with EMP alone, EMP with freeze-dried TNE and EMP with TNE and alginate. We made a series of observations that held true for each group. For clarity, we show this in Fig. 6 as the model, but the other groups showed similar features. In the EMP with TNE and alginate at the time of delivery, the EMP penetrated to the uppermost dermis as shown by the reflectance confocal microscopy images (Fig. 6). We observed a weak lipid signal from the stratum granulosum and stratum spinosum. This supported the hypothesis that the EMP retained some TNE coating but also released some Miglyol from the centre core of the emulsions (Fig. 6). Images from the dermal-epidermal junction revealed an obvious lipid signature that suggested that there was a considerable amount of Miglyol payload released at 40–60 μm deep in to skin. This was only observed in EMP assisted delivery. Thirty min after the initial application, TNE lipid signal was observed from the same EMP at the stratum spinosum and epidermaldermal junction at levels that were similar to the images just after application (data not shown).

This observation was reminiscent of the *in vitro* release observations shown in Fig. 3 and the delivery depth profiling in Figs. 4&5. Enhanced TNE delivery by using alginate coated EMP resulted in an increased amount of signal detected in the stratum spinosum and dermal-epidermal junction compared to the freeze-dried TNE coated EMP group that delivered the majority of the payload to the upper skin strata (Fig. 7). In summary, the profile of P20 TNE topical delivery can be controlled *via* EMP coating strategies.

3.4. Delivery and distribution of CaF in vivo

Volunteer imaging with MPM was limited in terms of time to image acquisition and the size of the imaging area. Therefore, we could not adopt the same experimental design as was possible with excised skin. That said, we were able to acquire penetration depth data and to examine some later time points in volunteers We applied alginate coated EMP (dry) -TNE (P20) formulation in volunteer's forearms and imaged the delivery profile by MPM with higher magnification (40×). We guided ourselves using NADH channel to identify the skin structure. Fig. 8 displays pseudo-coloured representative MPM images taken 15 min and 50 min after EMP-TNE was topically applied, along with TNE alone. CaF was minimally detected in TNE alone. At 15 min after application, EMP penetrated the surface of skin (Fig. 8) and some CaF from TNE core was released. This finding is aligned with our observations of the lipid core using CARS imaging (Fig. 6). There was very shallow delivery of CaF down to stratum granulosum (5 μm). This observation is also seen in results from CARS images (Fig. 6). By 50 min post application, the delivery profile had changed. The intense CaF signal initially seen outlining the EMP was observed to be less distinct and was detected deeper into the skin suggesting TNE diffusion away from the EMP over time. Images from the DEJ showing a strong signal from the TNE payload reaching 40–60 μm into the skin. This is a similar release profile to what we observed in our *ex vivo* experiments (Fig. 6) and was only observed with EMP-enhanced delivery.

The image analysis of MPM-FLIM (10× objective) signal correlated to these observations (Fig. 9). In summary, we observed the similar delivery profile as *ex vivo* in *in vivo*. In volunteers, our selection of coating strategy (alginate-dry coated EMP) enhanced the TNE delivery into viable epidermis.

4. Discussion

We have developed a novel platform where enhanced drug delivery into the skin can be achieved through a combination of EMP and TNE using both freeze drying and alginate co-formulations. The penetration of EMP into the skin results in enhanced delivery compared to topical application alone. In a simple mixture, EMP and TNE can be combined and freeze-dried for superficial payload delivery enhancement. EMP and TNE can also be formulated with cross-linked alginate resulting in a relatively uniform and continuous delivery profile deep within the viable epidermis. The results from *ex vivo* model experiments have shown the TNE core lipid was predominantly within the stratum corneum, with some apparent, but limited, penetrated into the upper viable epidermis when EMP was not coated with alginate. While if EMP was coated with alginate and freeze dried with TNE, the levels of DiI detected within the viable epidermis tended to be higher. Most importantly, lipophilic molecules can

be delivered to the viable epidermis in a well-controlled fashion. Similar delivery release profile was observed *in vivo* study. We applied *in vitro* and *ex vivo* proven EMP coating strategy with TNE to volunteers. MPM-FLIM images indicate early release of CaF from TNE as soon as EMP contacts to the skin surface. The fluorescent signal accumulates in viable epidermis as the time passes. This delivery release profile correlates to the results from *ex vivo* study. This potentially allows for the incorporation of a variety of therapeutic drugs or cosmeceuticals into TNE and delivered by EMP.

Nanoemulsions possess powerful nano-scale properties that make them attractive for diverse applications such as drug delivery, food supplements, nanoparticle synthesis and pharmaceutical formulation. With 40% of new therapeutic candidates and over 30% of new pipeline drugs showing poor water solubility, there is a great need for systems that are able to deliver the lipophilic molecules to the viable epidermis area where most biological targets are exhibited. Current examples of commercially available drugs encapsulated into nanoemulsions include Diprivan (Propofol) from AstraZeneca, Etomidate from B. Braun Melsungen, Lipotalon from Merckel and Cyclosporin A from Allergan.

For topical nanoemulsions, a gel-based anti-fungal drug was tested *in vitro* and *in vivo* suggesting better alternative to painful and nephrotoxic intravenous administration [16]. A hydrogel-thickened nanoemulsion system for topical therapy for arthritis, minor joint and muscle pain using soybean lecithin showed significant advantages over the control-gel suggesting suitable viscosity might be a promising carrier for topical delivery of lipophilic drugs [17]. Topical nanoemulsions can also be absorbed through hair follicles and sweat glands, but their role is almost negligible in most cases. However, there is little knowledge in nanoemulsion about controlling and predicting droplet size and opportunities for *ad hoc* control over surface properties are limited. Our TNE are produced by using to stabilize the droplets of emulsions and are well tolerated when they are cross-linked with EMP. Seeing as TNE can be formulated with rational changes to its surface and is able to encapsulate poorly water-soluble molecules, it holds great promise as a new drug delivery carrier. Chuan et al. (2012) co-delivered a model antigen and a lipophilic, anti-inflammatory drug, curcumin, *via* TNE to cells *in vitro* [18,19]. Our study is the first to use TNE for topical application. As EMP is shown to be a promising platform for field-directed enhanced permeability of the skin's physical barriers. Enhanced TNE delivery with EMP is well suited for the treatment of skin disease where drugs are applied to larger areas of skin.

Alginate has previously been used to improve the delivery and release characteristics of topically applied drugs although alginate has not been reported in the context of microneedle enhanced delivery [20]. Alginate has been investigated for use as a vehicle for antimicrobial agent delivery by Friedman et al. in 2013 [21]. Their results show that a chitosan-alginate nanoparticle had direct antimicrobial activity, but remained non-toxic, suggesting that this alginate-chitosan formulation could be used to treat dermatological conditions. Our results also show no apparent, immediate toxicity in living human skin. Together, these observations support the further investigation and development of this technology for topical application. We observed a controlled, relatively slow release profile from alginate coated EMP *in vitro* and in excised human skin. The freeze-dried approach resulted in a burst release profile that limited delivery to the superficial skin that was not observed with the

alginate formulation. In 2015, Ibrahim et al. reported the use of an alginate nanoparticle for topical ophthalmic delivery [22]. They observed a similar release profile in which their alginate nanoparticle slowly released brimonidine without an initial burst release profile. These findings support our observation and hypothesis that using crosslinked alginate is a viable means of controlling the release of TNE from EMP *in situ*.

We and others have investigated formulation effects on microneedle release profiles [23–26]. However, the vast majority of these studies, including ours, have been in mouse or rarely porcine skin. Very few if any studies have been done *in vivo* human skin with this focus. Although there are limitations to volunteer imaging, the data is valuable and relevant to the translation of novel topical delivery technologies.

5. Conclusions

This study demonstrates for the first time the use of a novel nanoparticle topical delivery enhancement strategy in volunteers. We characterized a peptide surfactant nanoparticle with a lipid core alone and in a series of dry formulations. These formulations were then applied to EMP so that the topical penetration of the TNE could be enhanced. These formulations showed controlled release patterns determined largely by crosslinking on the EMP. Experiments in living, but excised, human skin revealed promising penetration enhancement with EMP. MPM and CARS imaging results supported the hypothesis that this approach was minimally invasive and that the EMP-TNE combination effectively enhanced delivery to the deep viable epidermis. Volunteers treated with the EMP-TNE formulation showed no adverse effects and the MPM imaging results further demonstrated topical delivery enhancement. Together these results show that combing EMP with TNE can significantly improve topical delivery of problematic molecules to the deep viable epidermis in a minimally invasive manner. This system has broad utility in both medical and cosmetic fields.

Supplementary Material

Refer to Web version on PubMed Central for supplementary material.

Acknowledgements

References

[1]. Chan HK. Nanodrug particles and nanoformulations for drug delivery. Adv. Drug Deliv. Rev 2011;63(6):405. doi: 10.1016/j.addr.2011.05.006. [PubMed: 21601602]

[2]. Paudel KS, Milewski M, Swadley CL, Brogden NK, Ghosh P, Stinchcomb AL, Challenges and opportunities in dermal/transdermal delivery, Ther. Deliv 1 (1) (2010) 109–131 (PubMed PMID: 21132122; PubMed Central PMCID: PMC2995530). [PubMed: 21132122]

[3]. Labouta HI, Liu DC, Lin LL, Butler MK, Grice JE, Raphael AP, et al. , Gold nanoparticle penetration and reduced metabolism in human skin by toluene, Pharm. Res 28 (11) (2011) 2931–2944 Epub 2011/08/13 10.1007/s11095-011-0561-z (PubMed PMID: 21833791). [PubMed: 21833791]

[4]. Mason TG, Wilking JN, Meleson K, Chang CB, Graves SM, Nanoemulsions: formation, structure, and physical properties, J. Phys. Condens. Matter 18 (41) (2006) R635–R666, 10.1088/0953-8984/18/41/r01.

[5]. Hormann K, Zimmer A, Drug delivery and drug targeting with parenteral lipid nanoemulsions - a review, J. Control. Release 223 (2016) 85–98, 10.1016/j.jconrel.2015.12.016 (PubMed PMID: 26699427). [PubMed: 26699427]

[6]. Sainsbury F, Zeng B, Middelberg APJ, Towards designer nanoemulsions for precision delivery of therapeutics, Curr. Opin. Chem. Eng. 4 (0) (2014) 11–17, 10.1016/j.coche.2013.12.007.

[7]. Middelberg AP, Radke CJ, Blanch HW, Peptide interfacial adsorption is kinetically limited by the thermodynamic stability of self association, Proc. Natl. Acad. Sci. U. S. A 97 (10) (2000) 5054–5059, 10.1073/pnas.080042597 (PubMed PMID: 10792027; PubMed Central PMCID: PMC25780). [PubMed: 10792027]

[8]. Malcolm AS, Dexter AF, Katakdhond JA, Karakashev SI, Nguyen AV, Middelberg APJ, Tuneable control of interfacial rheology and emulsion coalescence, Chemphyschem 10 (5) (2009) 778–781, 10.1002/cphc.200900023 (PubMed PMID: WOS:000264774300007). [PubMed: 19253928]

[9]. Middelberg AP, Dimitrijev-Dwyer M, A designed biosurfactant protein for switchable foam control, ChemPhysChem 12 (8) (2011) 1426–1429, 10.1002/cphc.201100082 (PubMed PMID: 21365736). [PubMed: 21365736]

[10]. Zeng BJ, Chuan YP, O'Sullivan B, Caminschi I, Lahoud MH, Thomas R, et al. , Receptor-specific delivery of protein antigen to dendritic cells by a nanoemulsion formed using top-down non-covalent click self-assembly, Small (2013), 10.1002/smll.201300078 (PubMed PMID: 23606503).

[11]. Raphael AP, Primiero CA, Lin LL, Smith RF, Dyer P, Soyer HP, et al. , High aspect ratio elongated microparticles for enhanced topical drug delivery in human volunteers, Adv. Healthc. Mater 3 (6) (2014) 860–866, 10.1002/adhm.201300517 (PubMed PMID: 24421280). [PubMed: 24421280]

[12]. Raphael AP, Sisney JP, Liu DC, Prow TW, Enhanced delivery of nano- and submicron particles using elongated microparticles, Curr. Drug Deliv 12 (1) (2015) 78–85 (PubMed PMID: 25176162). [PubMed: 25176162]

[13]. Rudd PA, Raphael AP, Yamada M, Nufer KL, Gardner J, Le TT, et al. , Effective cutaneous vaccination using an inactivated chikungunya virus vaccine delivered by Foroderm, Vaccine 33 (39) (2015) 5172–5180, 10.1016/j.vaccine.2015.07.099 (PubMed PMID: 26296498). [PubMed: 26296498]

[14]. Raphael AP, Primiero CA, Ansaldo AB, Keates HL, Soyer HP, Prow TW, Elongate microparticles for enhanced drug delivery to ex vivo and in vivo pig skin, J. Control. Release 172 (1) (2013) 96–104, 10.1016/j.jconrel.2013.07.025 (PubMed PMID: 23933236). [PubMed: 23933236]

[15]. Le TT, Yue S, Cheng JX, Shedding new light on lipid biology with coherent anti-Stokes Raman scattering microscopy, J. Lipid Res 51 (11) (2010) 3091–3102, 10.1194/jlr.R008730 (PubMed PMID: 20713649; PubMed Central PMCID: PMC2952550). [PubMed: 20713649]

[16]. Hussain A, Samad A, Singh SK, Ahsan MN, Haque MW, Faruk A, et al. , Nanoemulsion gel-based topical delivery of an antifungal drug: in vitro activity and in vivo evaluation, Drug Deliv 23 (2) (2016) 652–667, 10.3109/10717544.2014.933284 (PubMed PMID: 25013957).

[17]. Mou D, Chen H, Du D, Mao C, Wan J, Xu H, et al. , Hydrogel-thickened nanoemulsion system for topical delivery of lipophilic drugs, Int. J. Pharm 353 (1–2) (2008) 270–276, 10.1016/j.ijpharm.2007.11.051 (PubMed PMID: 18215479). [PubMed: 18215479]

[18]. Chuan YP, Zeng BY, O'Sullivan B, Thomas R, Middelberg AP, Co-delivery of antigen and a lipophilic anti-inflammatory drug to cells via a tailorable nanocarrier emulsion, J. Colloid Interface Sci 368 (1) (2012) 616–624 Epub 2011/12/14 10.1016/j.jcis.2011.11.014 (PubMed PMID: 22153851). [PubMed: 22153851]

[19]. Tayeb HH, Piantavigna S, Howard CB, Nouwens A, Mahler SM, Middelberg APJ, et al. , Insights into the interfacial structure-function of poly (ethylene glycol)-decorated peptide-stabilised nanoscale emulsions, Soft Matter 13 (43) (2017) 7953–7961 Epub 2017/10/19 10.1039/c7sm01614j (PubMed PMID: 29038804).

[20]. Goyal R, Macri LK, Kaplan HM, Kohn J, Nanoparticles and nanofibers for topical drug delivery, J. Control Release (2015), 10.1016/j.jconrel.2015.10.049 (PubMed PMID: 26518723; PubMed Central PMCID: PMCPMC4896846).

[21]. Friedman AJ, Phan J, Schairer DO, Champer J, Qin M, Pirouz A, et al. , Antimicrobial and anti-inflammatory activity of chitosan-alginate nanoparticles: a targeted therapy for cutaneous pathogens, J. Invest. Dermatol 133 (5) (2013) 1231–1239, 10.1038/jid.2012.399 (PubMed PMID: 23190896; PubMed Central PMCID: PMCPMC3631294). [PubMed: 23190896]

[22]. Ibrahim MM, Abd-Elgawad AH, Soliman OA, Jablonski MM, Natural bioadhesive biodegradable nanoparticle-based topical ophthalmic formulations for management of glaucoma, Transl. Vis. Sci. Technol 4 (3) (2015) 12, 10.1167/tvst.4.3.12 (PubMed PMID: 26175958; PubMed Central PMCID: PMCPMC4497485).

[23]. Gill HS, Prausnitz MR, Coated microneedles for transdermal delivery, J. Control Release 117 (2) (2007) 227–237, 10.1016/j.jconrel.2006.10.017 (PubMed PMID: 17169459; PubMed Central PMCID: PMCPMC1853346). [PubMed: 17169459]

[24]. McCrudden MT, Alkilani AZ, McCrudden CM, McAlister E, McCarthy HO, Woolfson AD, et al. , Design and physicochemical characterisation of novel dissolving polymeric microneedle arrays for transdermal delivery of high dose, low molecular weight drugs, J. Control Release 180 (2014) 71–80, 10.1016/j.jconrel.2014.02.007 (PubMed PMID: 24556420; PubMed Central PMCID: PMCPMC4034161). [PubMed: 24556420]

[25]. Raphael AP, Crichton ML, Falconer RJ, Meliga S, Chen X, Fernando GJ, et al. , Formulations for microprojection/microneedle vaccine delivery: structure, strength and release profiles, J. Control. Release 225 (2016) 40–52, 10.1016/j.jconrel.2016.01.027 (PubMed PMID: 26795684). [PubMed: 26795684]

[26]. Yucel T, Lovett ML, Kaplan DL, Silk-based biomaterials for sustained drug delivery, J. Control Release 190 (2014) 381–397, 10.1016/j.jconrel.2014.05.059 (PubMed PMID: 24910193; PubMed Central PMCID: PMCPMC4142080). [PubMed: 24910193]
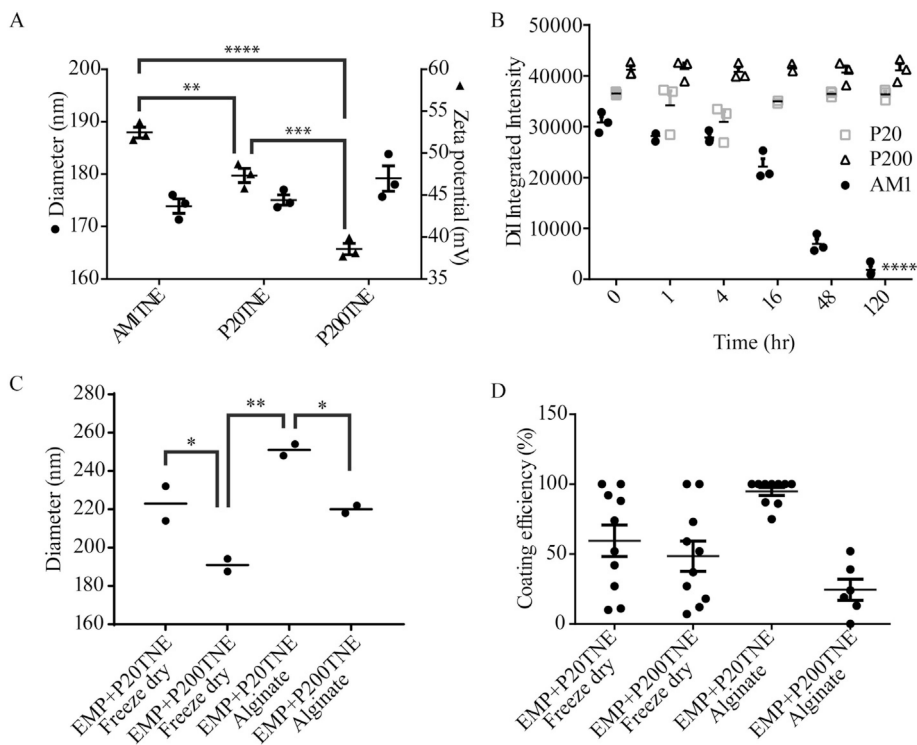
Fig. 1.

Tailorable nano-size emulsion (TNE) characterisation and keratinocyte toxicity. The diameter (nm; circles) and zeta potential (mV; triangles) of three TNE formulations are shown in Panel A, including AM1 alone (AM1TNE), with 20 μM of DAMP4-PEG (P20TNE) and 200 μM of DAMP4-PEG (P200TNE). The diameter significantly decreases as concentration of PEG increases. The DiI retention by TNE is shown in Panel B as a percentage of the encapsulated DiI signal at the time of emulsification. DiI was released from encapsulated AM1TNE after 16 h. Whereas DiI from P20 and P200 remained similar within the TNE after 5 days. Panel C shows the diameter of the formulations after release from EMP. For comparison, see the diameter (nm) of unbound TNE in Panel A. Freeze dried P20/P200 (Freeze dry) had no alginate or cross-linking between TNE and EMP. Alginate followed by crosslinking TNE onto EMP are also shown in Panel C (Alginate). All of the released complexes between TNE and EMP increased in radius with respect to the starting material. The P20TNE with alginate showed the largest increase after release at 23%. The coating efficiency was measured from the Coherent Anti-Stoke Raman Spectroscopy images of TNE coated EMP (Panel D). The continuity of lipid intensity was measured and is expressed as a percentage. Values represent the mean of replicates ± standard deviation. Statistical analyses were performed using an analysis of variance (ANOVA) followed by Tukey's *post hoc* test. **indicates $p < .05$; *** indicates $p < .001$; and ****indicates $p < .0001$.
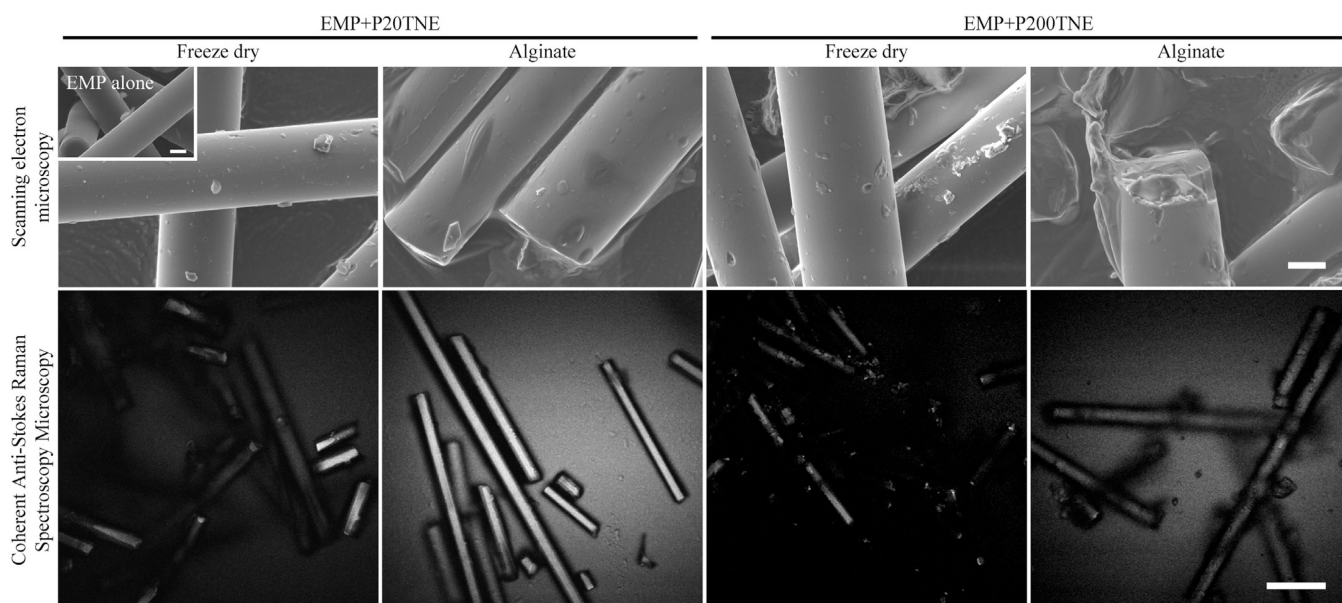
Fig. 2.
In vitro dry coating morphology. Scanning electron microscopy was used to image EMP coated with P20TNE or P200TNE using freeze drying or cross-linked alginate. The cross-linked alginate-coated EMP appeared to have a thin layer of continuous coating over the surface. The freeze-dried samples had large aggregates on and around the EMP. Coherent Anti-Stokes Raman Scattering microscopy images revealed a strong lipid-based signal on the EMP coated with P20TNE and alginate. The other samples had weaker signal and irregular aggregates. Bars indicate 5 μm and 25 μm for scanning electron microscopy and Coherent Anti-Stokes Raman Scattering microscopy, respectively.
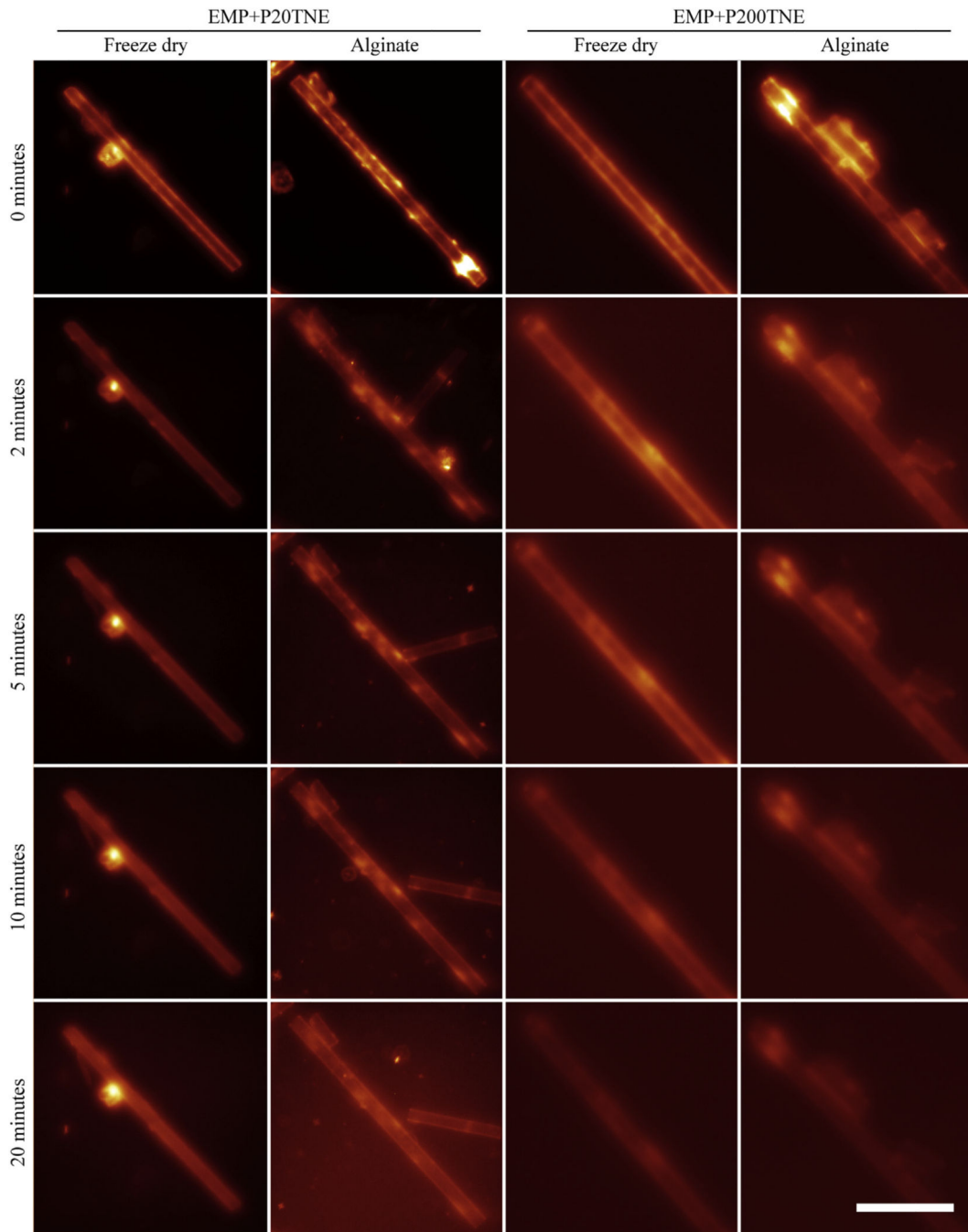
Fig. 3.

In vitro release of TNE from dry coated EMP. EMP were imaged over time with fluorescence microscopy. The EMP were coated with either P20TNE or P200TNE containing DiI as a lipophilic fluorescent tracer. The time series showed that the freeze dried EMP coated with P20TNE immediately decreased in intensity after being exposed to PBS. Some of the large aggregates did not appear to change in intensity or size over the 20 min observation period. The EMP coated with P20TNE and alginate appeared to have a slower release profile and the surface coating changes can be seen over 20 min. Both the

P200TNE groups appeared to immediately release the majority of the coating. The EMP surface coating in the P200TNE groups did show any apparent differences over the time observed. Bar indicates 50 μm.
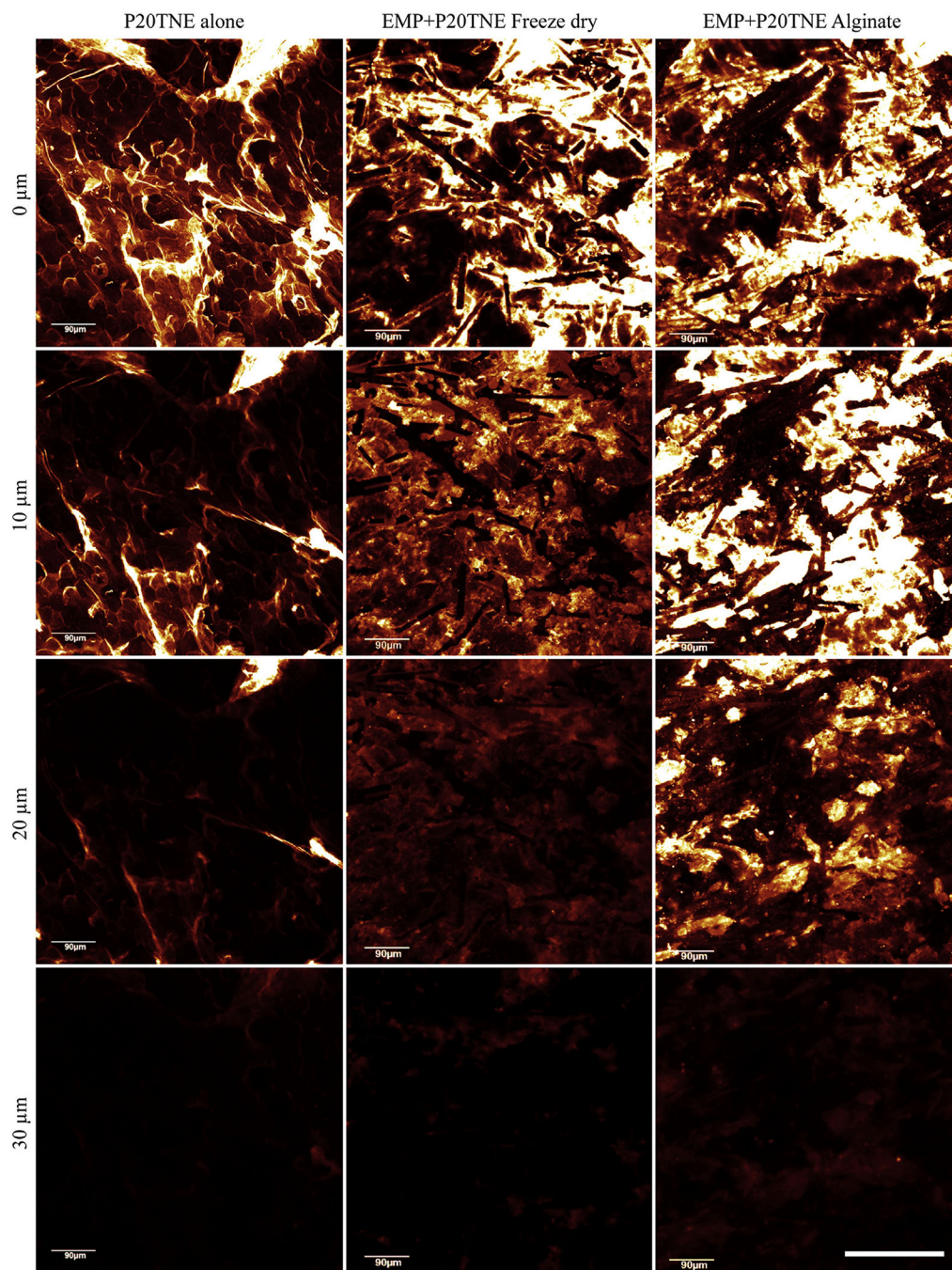
Fig. 4.

Topical delivery of TNE was enhanced by EMP and alginate in thawed excised human skin after 30 min. Confocal microscopy images showing DiI containing P20TNE delivery at the surface (0 μm), 10, 20 and 30 μm deep in human skin. Treatment groups included no EMP (P20TNE alone), EMP coated with P20TNE freeze dried (EMP + P20TNE Freeze dry) and EMP coated with P20TNE with alginate (EMP + P20TNE Alginate). The P20TNE alone appears to partition in the stratum corneum and furrows. The EMP coated with P20TNE using freeze drying were capable of delivering detectable DiI to the upper viable epidermis

whereas the alginate group was detected around the dermal-epidermal junction at > 30 μm deep. Bar indicates 200 μm.
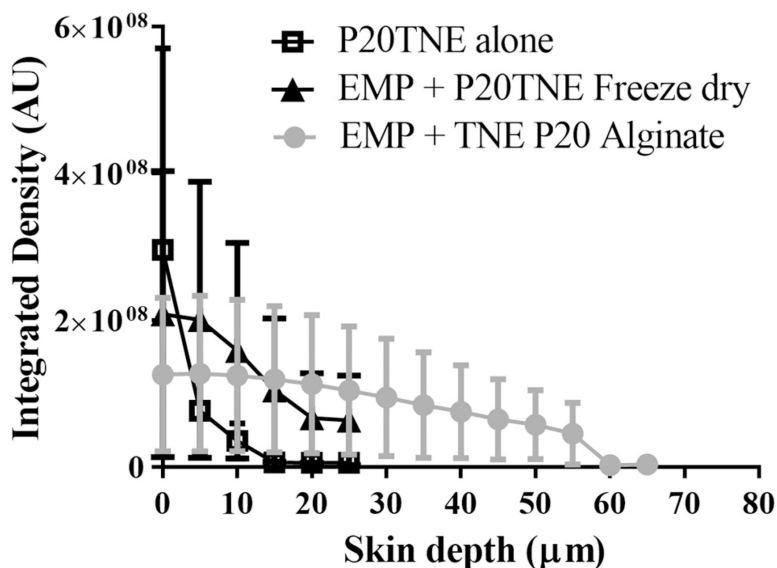
Fig. 5.
Image analysis of TNE delivery in freshly excised human skin after 30 min incubation. The fluorescence intensity profiles were determined by image analysis of z-stacks taken from TNE treated human skin. These results showed that the P20TNE alone treatment resulted in detectable signal only in the stratum corneum (< 10 μm deep). The EMP coated with P20TNE showed different delivery profiles depending on the dry coating strategy. Treating with the freeze-dried material resulted in a shallow release profile with high intensity signal from the stratum corneum and upper viable epidermis (< 15 μm deep). The alginate coated material showed a consistent level of delivery enhancement to the dermal-epidermal junction (30–50 μm deep). The experiment was performed in 3 different pieces of donor skin. P20TNE alone has delectable values up to 10 μm deep. EMP + P20TNE freeze dry was detected up to 25 μm. EMP + P20TNE alginate has detectable values up to 55 μm. No significance was found at < 25 μm deep. There was no detectable signal > 25 μm deep in the P20TNE alone or EMP + P20TNE Freeze dry groups. Only signal from EMP + TNEP20 Alginate was detected deeper than 25 μm.
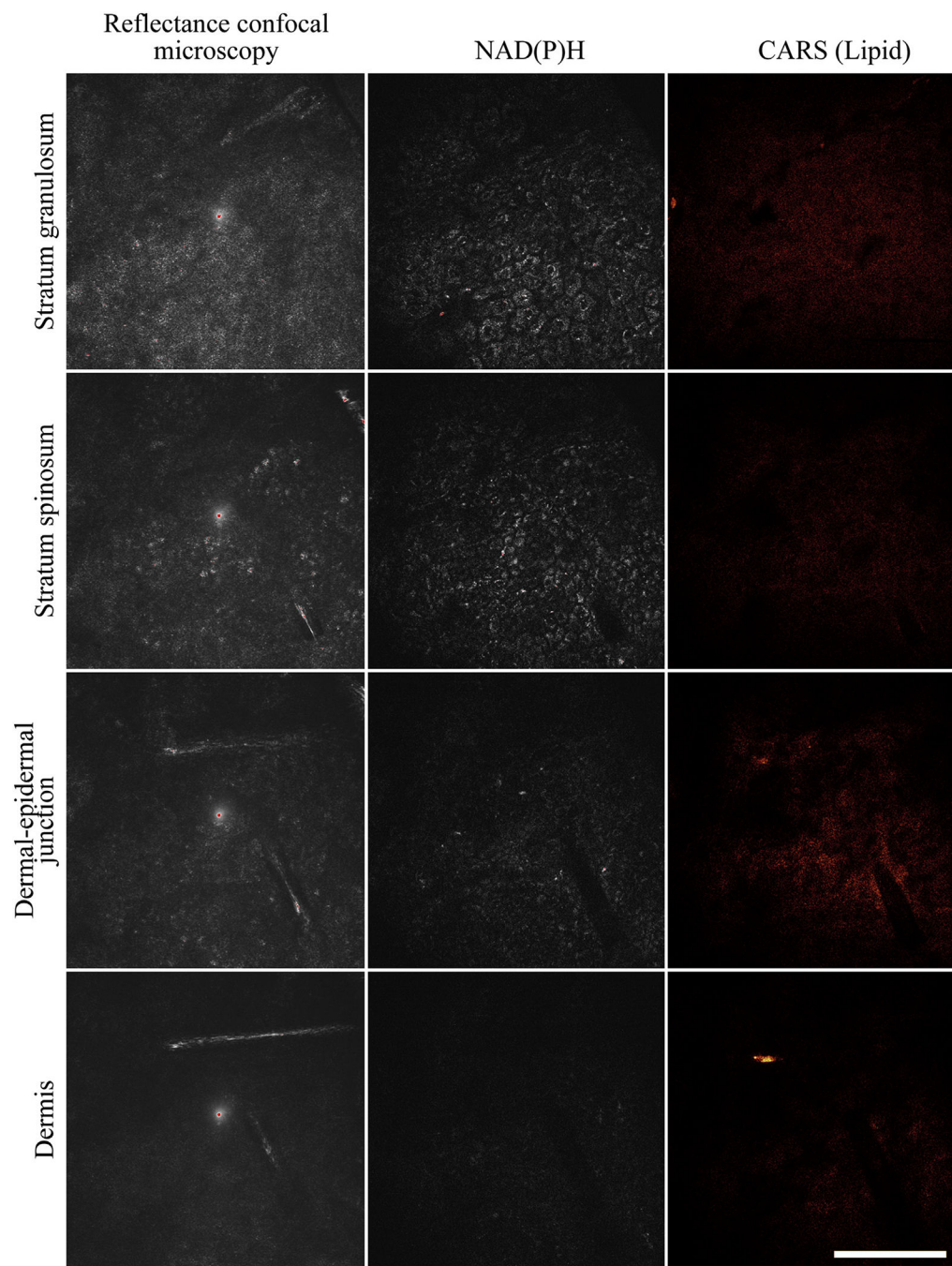
Fig. 6.
Depth effects of EMP coated with P20TNE using alginate by reflectance confocal microscopy, NAD(P)H imaging and CARS imaging for lipid signal. Reflectance confocal microscopy showed the presence of EMP through the skin. The NAD(P)H imaging revealed a dark halo around the EMP suggesting that there was a gap between the EMP and viable skin. CARS imaging showed the presence of lipid signal hot spots primarily at the surface and dermal-epidermal junction. Bar indicates 50 μm.
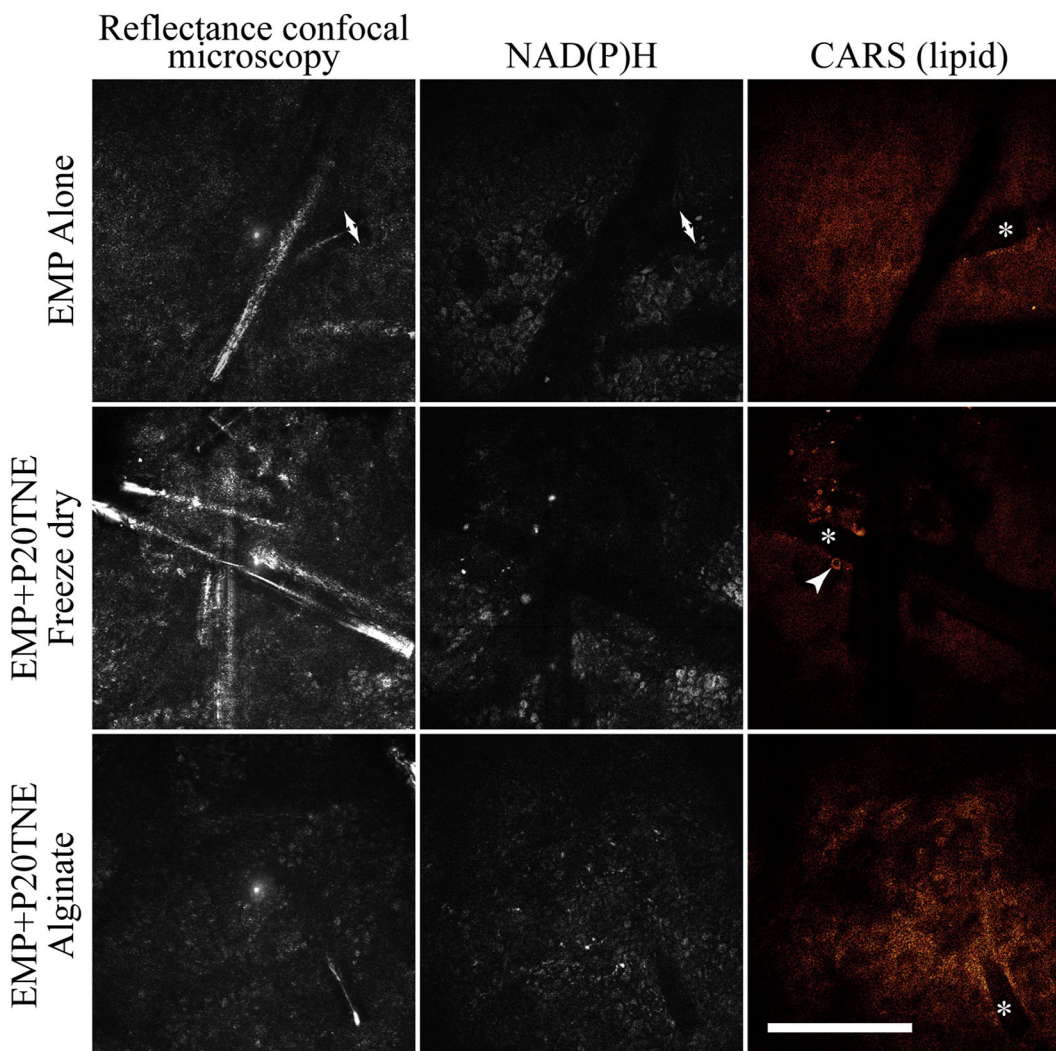
Fig. 7.
Effects of EMP enhanced delivery of P20TNE within the dermal-epidermal junction after 30 min. All three imaging modalities are shown at the same depth. Reflectance confocal microscopy was used to identify the skin strata and EMP. The EMP diameter is highlighted with double arrow heads in both the reflectance and the NAD(P)H images. Both reflectance and NAD(P)H images show similar halos around the EMP regardless of EMP coating. This suggests that there is a zone of cell death or oedema around one cell diameter around the EMP. The CARS imaging revealed more intense lipid signal with EMP coated with P20TNE and alginate than either of the other groups. CARS imaging also confirmed that the large aggregates in the P20TNE freeze dried groups contain high levels of lipid that did not dissipate over 30 min. The images for P20TNE with alginate are the same area as shown in Fig. 6, but after 30 min. Bar indicates 50 μm.
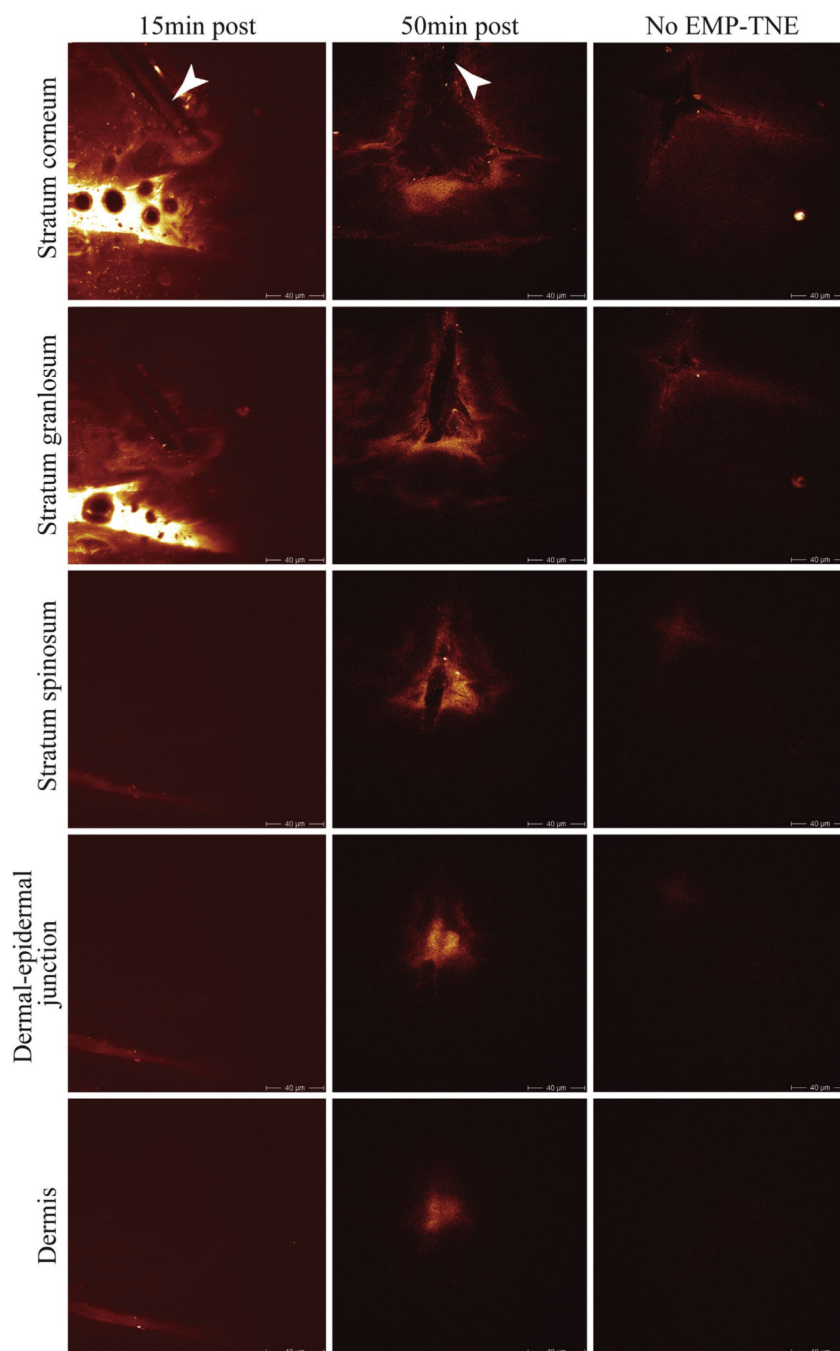
Fig. 8.

In vivo pseudo coloured MPM images of volunteer skin at various depth (40×), 15 min and 50 min after the topical application of EMP-TNE (P20) formulation. Images from NADH channel to identify the skin structure (images are not shown). MPM images showing CaF containing P20TNE delivery at each skin strata in volunteer skin. At early point (15 min), majority of TNE stayed the surface of the skin. 50 min after the application, more intense TNE signal released from EMP was detected at viable dermal-epidermal junction. Bar indicates 40 μm.
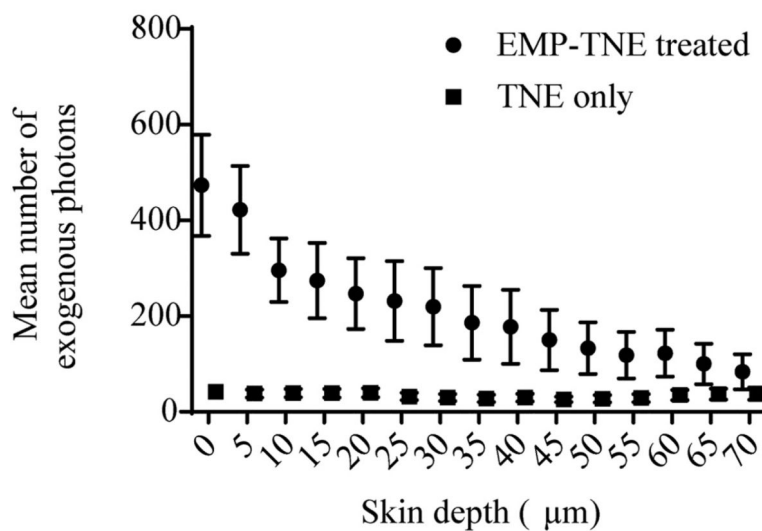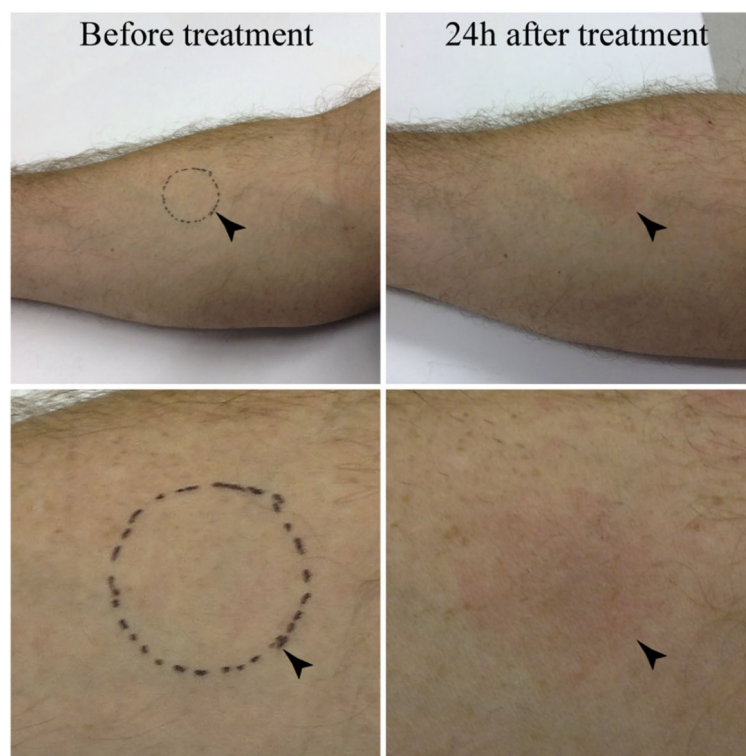
Fig. 9.
FLIM Image analysis of TNE delivery *in vivo* after 30 min of application (10× objective). The graph shows significant improvement in TNE delivery with EMP in comparison to TNE alone ($p < .0001$). The effective of delivery was claculated by mean number of exogenous (EMP-TNE signals that are normalised to EMP alone) photons (y-axis). Skin depth (μm) is shown in x-axis. There is minimal delivery of CaF from TNE into skin without EMP (TNE only). EMP-TNE delivery resulted in a release profile with high intensity signal from stratum corneum to upper viable epidermis (> 30 μm). Mean values with standard

deviation of 3 volunteers with 3 individual imaging sites per volunteer per group are shown. Significance was determined with a two-way ANOVA and Mann-Whitney *U* test.